Galactic Chemical Evolution Models for Stable and Short-lived Nuclides

T. Kaur[1], D. Romano[2], M. Molero[3,4], A. Vasini[3,4], and F. Matteucci[3,4,5]

[1] Department of Physics, Panjab University, Chandigarh, 160014, India
[2] INAF, Osservatorio di Astrofisica e Scienza dello Spazio, Via Gobetti 93/3, 40129 Bologna, Italy
[3] Dipartimento di Fisica, Sezione di Astronomia, Università degli studi di Trieste, Via G.B. Tiepolo 11, I-34143 Trieste, Italy
[4] INAF, Osservatorio Astronomico di Trieste, Via Tiepolo 11, I-34131 Trieste, Italy
[5] INFN Sezione di Trieste, via Valerio 2, 34134 Trieste, Italy
e-mail: `tejpreetkaur95@gmail.com`

Abstract. This work discusses different Galactic chemical evolution (GCE) models and their use to decipher the evolution of stable and unstable nuclides in the Galaxy. In this paper, we discuss GCE models for ^{7}Li, radioactive nuclides ^{26}Al and ^{60}Fe, neutron capture elements, Eu and Ba, along with the impact of and the rotational yields' on the chemical evolution. A sample of 3210 open cluster (OC) stars and field stars is analysed to find the ^{7}Li abundance in the Galaxy. The observations are then compared with the predicted trends for ^{7}Li from the GCE models. Further, the galactic abundance of short-lived radionuclides, ^{26}Al and ^{60}Fe is predicted by the GCE models. The GCE model predictions suggest new constraints for the nova rate and propose novae as the main producers of ^{7}Li and ^{26}Al in the Galaxy. The GCE models for neutron capture elements in the dwarf and ultra dwarf galaxies investigated the role of merging neutron stars and magneto-rotational driven supernovae in producing r-process (rapid neutron capture) elements like Eu. For Ba, which is an s-process (slow neutron capture) element, nucleosynthesis from Low and intermediate stars is also considered. Further, the impact of rotational yields for massive stars on the evolutionary history of the Galaxy is studied by developing GCE models with yields of the massive stars with rotational velocities of 0, 150 and 300 km s^{-1}, and the [Fe/H] values of 0, -1, -2, and -3. The results for the G-dwarf distribution for all of the models with different yield sets show broad agreement with the observations with deviation in the low metallicity regime.

Key words. Stars: abundances – Galaxy: evolution – Galaxy: radionuclides – Galaxy: open clusters – Galaxy: abundances

1. Introduction

The Galactic chemical evolution (GCE) models are developed to understand the temporal and spatial evolution of elements in the Milky Way Galaxy and other galaxies of varied morphology (Timmes et al. 1995; Matteucci & Francois 1989; Chiappini et al. 2001; Matteucci 2001; Sahijpal & Kaur 2018; Matteucci 2021). It is essential to understand

the chemical evolution of the galaxies because it is well established that the elements observed in the present-day universe were not created in a single instant but evolved over time. Except for Hydrogen, Helium and Lithium, all heavier elements observed in the present-day universe are formed by thermonuclear reactions inside the stars in a complex process of Stellar nucleosynthesis. The final elemental yields of any star result from a series of nuclear processes like proton-proton (pp)-chain, Carbon, Nitrogen & Oxygen (CNO)-cycle, neutron (slow & fast) capture, proton capture etc. (Pagel 2009).These nuclear processes are sensitive to the temperature and pressure of the stellar interior, which are further decided by the star's mass, metallicity and age. Stars can be widely categorized as Low and intermediate mass stars (LIMS) (< 10 $M_\odot$) and massive stars (>11$M_\odot$). The LIMS evolve as Asymptotic giant branch stars (AGB) and Red giant (RG) phases and die as white dwarfs over a long life-span of the order of billion years. On the other hand, massive stars evolve over a very short life span (a few million years) as core-collapse Supernovae and end their life as Neutron stars or Black holes. Some LIMS evolve as binary stars and explode as Supernova Ia and Novae [1]. There are also observations of the merger of Neutron stars and Black Holes events by Gravitational waves. The former can be the potential contributor to the Galaxy's heavy r-process elements. When synthesized elements in various stellar circumstances are ejected into the Interstellar medium (ISM), the ISM gas's metallicity increases. When the metal-rich ISM gas cools down, it forms new generations of stars with higher metallicity. In this way, each generation of stars contributes to the chemical enrichment of the Galaxy.

---

[1] These are close binary systems in which a white dwarf accretes matter from a main sequence or giant companion. When the bottom of the accreted envelope reaches temperatures of the order of 10^8 K, a thermonuclear runaway develops and ^{7}Li is produced. The outburst does not destroy the system and another cycle starts after the ejection of the envelope (e.g., José & Hernanz 2007, and references therein).

With the galactic archaeology data available for different parts of the Milky Way Galaxy, there is a better understanding of the solar neighbourhood, the Halo, Bulge, and inner and outer disc of the Galaxy. The data on [α/Fe] vs [Fe/H] indicates that the Galaxy's Halo, Bulge, and thick and thin disc components formed over different timescales. GCE models simulate it correctly by including various galactic components' different kinematic and chemical properties. Also, with the availability of the chemical data from the neighbouring galaxies, the GCE models successfully understand the history of star formation and accretion for galaxies of other morphology. The results for the abundance of stable and radioactive nuclides obtained from GCE models are compared with the observational data. Hence, GCE models predict the Galaxy's formation and evolution history by fulfilling the constraints offered by the present-day observables (Chiappini et al. 1997).

In the following sections, we discuss the GCE models and their predictions for stable and radioactive elements in the Milky way Galaxy along with r-process elements in the dwarf galaxies. In section 2.1, results are presented to understand the ^{7}Li enrichment in the Galaxy. Here, ^{7}Li abundance is determined from a large sample belonging to open clusters and field stars. The abundance trends for Li are then obtained as a function of metallicity and the galactocentric radius from the parallel GCE models. Section 2.2 discusses the evolution of neutron-capture elements in local dwarf galaxies by incorporating various nucleosynthesis prescriptions. The contribution of the slow and rapid neutron capture processes is also investigated to understand the observed trends for Eu and Ba in dwarf galaxies. Section 2.3 presents the results for the GCE model to estimate the short-lived radionuclides, ^{26}Al and ^{60}Fe, in the Milky Way Galaxy. The model explains the Gamma-ray observed mass of ^{26}Al from the inner galactic region from the GCE model of Bulge and inner disc. Also, the results predict the mass estimates for ^{60}Fe in the Galaxy. In 2.4, the GCE models to understand the impact of massive stars on the evolution of the Milky Way are discussed. The incorpora-

tion of the rotation in massive stars results in higher yields of the CNO cycle products because of the enhanced mixing in different stellar layers. The GCE models predict the trends for G–dwarf distribution with rotating and non-rotating yields of massive stars. Further, in section 3, we discuss the summary and conclusion.

2. Chemical Evolution Models

Different modelling approaches can be used to develop the GCE models i.e., integro-differential equation (Matteucci & Francois 1989), N body chemo–dynamical (Kobayashi & Nakasato 2011; Minchev et al. 2013) and direct Monte carlo approach (Alibés et al. 2001; Sahijpal & Gupta 2013; Sahijpal & Kaur 2018). The chemodynamical models evolve the Galaxy from the cosmological model involving the dynamics. Here, we will discuss the numerical approach to developing GCE models. Independent of the method used to develop numerical GCE models, the underlying treatment mainly depends upon the accretion of gas, star formation history and gas flows in and out of the Galaxy. An exponentially decaying law generally describes the accretion of the gas over the galactic time scale (Matteucci & Francois 1989; Timmes et al. 1995; Prantzos & Aubert 1995; Chiappini et al. 1997). The different components, viz., Halo, thick and thin disc of the Galaxy in such a system can be more commonly formed by parallel or serial formations accretion scenarios (Matteucci 2021). In the serial formation scenario, galactic components forms on a continuous temporal scale which can occur in one, two or three–infall episodes (Matteucci & Francois 1989; Burkert et al. 1992). In the case of parallel formation, different galactic components form simultaneously with varying rates of accretion (Pardi et al. 1995; Grisoni et al. 2019). The metallicity of the infalling material also plays a crucial role in the chemical evolution of the ISM (Koeppen & Arimoto 1990; Pagel 2009). The accreting gas is supposed to have had primordial composition during the early growth. It can have slightly increased value with time as there are observations of the accretion of metal–rich high–velocity clouds onto the Galaxy (Wakker et al. 1999).

The star formation history in the Galaxy mainly depends upon the star formation rate (SFR) and initial mass function (IMF) prevalent in the Galaxy. SFR decides the rate of conversion of the accreted gas into the stars and mainly depends upon the gas surface mass density (Kennicutt 1998).The IMF gives the distribution of the stars with their mass and is a power law distribution (Scalo 1986).The exponent of the distribution can have single or multiple slopes in different parts of the mass spectra(Salpeter 1955; Kroupa 1998). Empirical relations formalism exists for both primarily based on the star-forming regions' observations. The gas outflows account for the gas lost from the Galaxy by galactic winds and are considered to be proportional to the SFR in the Galaxy (Matteucci 2001). The stars formed in the Galaxy enrich the ISM with their yields at the end of their life span. In the case of the GCE models with instant-recycling approximation, the lifetime of the stars is considered to be zero, and the stars contribute their yields into the ISM at the same time when they are born. This approximation is justified for massive stars for which the life span is short compared to the galactic time scale, but the low mass stars can cause discrepancies in the predicted results of the GCE models. Different stellar yield sets are available from various groups in the literature for stars of different masses and metallicities (Woosley & Weaver 1995; Woosley & Heger 2006; Karakas 2010; Limongi & Chieffi 2018). LIMS are the main producers of the Galaxy's C, N and s-process elements. Mainly alpha elements, along with some Fe-peak elements and r-process elements, are produced in the massive stars. SNIa is the main contributor of Iron in the Galaxy. The delay time in the occurrence of the SNIa is the main reason for the higher $[\alpha/Fe]$ in the early period of the Galaxy evolution (Greggio 2005). The stellar yields play a significant role in the GCE model's prediction for abundance trends. However, the stellar yields are also subject to many uncertainties because of the continuous revisions in understanding processes in the stellar interiors and nuclear reaction rates.
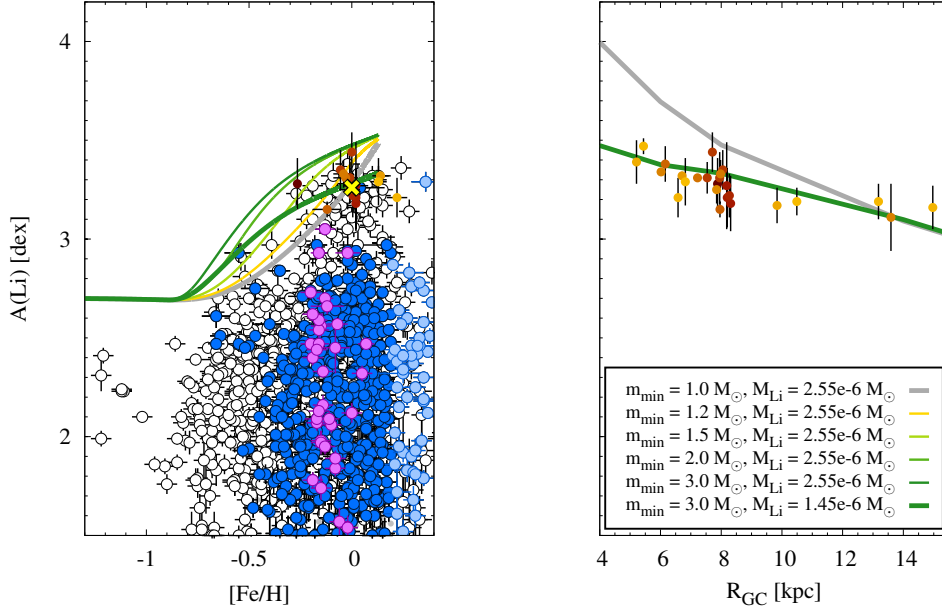
Fig. 1. Behaviour of $A(^7\text{Li})$ as a function of [Fe/H] in the local thin disc *(left panel)* and as a function of the galactocentric distance at the present time *(right panel)*. Lithium measurements for field low-α, metal-rich α-rich, and super metal-rich solar-α stars from GES iDR6 are shown as blue, magenta, and light blue circles, respectively (left panel only); empty circles represent stars without chemical membership that were attributed to the thin disc according to their kinematics. Small filled circles are average maximum ^7Li abundances (see Romano et al. 2021, for a definition of this quantity) for OCs with colour-coding according to the cluster's age (yellow for older clusters, brown for younger ones). Only clusters with ages < 2 Gyr are shown. The lines are the predictions of GCE models in which the mass range of primary stars entering the formation of nova systems is reduced from 1–8 $M_\odot$ to 3–8 $M_\odot$ (see legend in the right-hand panel). The predicted current nova outburst rate is kept fixed. The total amount of ^7Li ejected by each nova during its lifetime (dubbed M_{Li}) is also listed in the legend. Figure from Romano et al. (2021).

2.1. The Galactic lithium gradient

The main isotope of lithium (^7Li) is produced in non-negligible amounts during Big Bang nucleosynthesis (BBN; e.g., Steigman 2007). Its abundance in the ISM then increases as time goes by, in spite of the fact that $^7\text{Li}(p, \alpha)^4\text{He}$ reactions easily burn it inside stars wherever the temperature exceeds about 2.5×10^6 K.

In order to explain the increase of $A(^7\text{Li})^2$ from its primordial value – $A(^7\text{Li})_P^{\text{obs}} \simeq 2.2$ dex according to observational estimates (Spite & Spite 1982; Bonifacio & Molaro 1997) or $A(^7\text{Li})_P^{\text{th}} \simeq 2.7$ dex in the standard BBN scenario (e.g., Pitrou et al. 2018) – to that observed in meteorites and young T Tauri stars – $A(^7\text{Li}) \simeq 3.3$ (see, e.g., Lodders et al. 2009) – chemical evolution modelers have invoked ^7Li production from low-mass C-stars,

---

[2] In the usual spectroscopic notation, $A(^7\text{Li}) = 12 + \log(N_{\text{Li}}/N_{\text{H}})$, where N_{Li} and N_{H} are, respectively, the abundances of ^7Li and H by number.

massive AGB stars, core-collapse supernova precursors, cosmic rays and/or nova systems (D'Antona & Matteucci 1991; Matteucci et al. 1995; Romano et al. 1999, 2001; Travaglio et al. 2001). Being clear that the late, steep rise off the primordial 'Spite plateau' must be due to some long-lived source, novae have been proposed as major ^{7}Li factories (Romano et al. 1999; Izzo et al. 2015).

Our ability to characterize ^{7}Li producers, however, rests on our capacity of defining the upper envelope of the observations in the $A(^7\text{Li})$–[Fe/H] plane under the assumption that it traces the ^{7}Li enrichment history of the ISM. As already mentioned, ^{7}Li is easily destroyed inside the stars at relatively low temperatures; for instance, $A(^7\text{Li})$ is around 3.3 dex in meteorites (which do not suffer any ^{7}Li depletion process after their formation), but it is about 1 dex in the Sun (e.g., Asplund et al. 2009). Therefore, while the mean values of the highest ^{7}Li abundances in bins of metallicity are commonly used as appropriate indicators, it should be kept in mind that these could represent only lower limits to the true ISM ^{7}Li abundance.

It has been suggested that super-solar metallicity stars might trace a decrease of the ^{7}Li abundance in the local ISM (Delgado Mena et al. 2015; Guiglion et al. 2016; Fu et al. 2018). Some reduction of the stellar yields, contamination from thick-disc stars, or radial migration have been suggested to explain the odd decreasing trend inferred from the observations (Prantzos et al. 2017; Fu et al. 2018; Grisoni et al. 2019; Guiglion et al. 2019). Further observational studies, however, do not confirm the claims of decreasing $A(^7\text{Li})$ for [Fe/H] > 0. In the following, we report briefly on the results from the fifth and sixth internal data releases (iDR5 and iDR6) of the *Gaia*-ESO Survey (GES; Gilmore et al. 2012; Randich et al. 2013). The results are discussed at length in Randich et al. (2020) and Romano et al. (2021).

We use ^{7}Li abundances and stellar parameters determined by the GES Consortium (GES iDR6) for pre-main-sequence, main-sequence, turn-off, and sub-giant stars observed with the multi-object optical fibre facility FLAMES (Pasquini et al. 2002) in the Milky Way field and in open clusters (OCs). The sample stars are cross-matched with the Gaia Early Data Release 3 (EDR3) catalogue (Gaia Collaboration et al. 2016, 2021) to obtain a full chemodynamical characterisation (see Romano et al. 2021, for details).

The final sample of field stars consists of 3210 objects with $5300 \le T_{\text{eff}}/\text{K} \le 7000$, $3.5 \le \log g \le 4.6$, $-1.5 < $ [Fe/H] $ < +0.5$, S/N ≥ 50, $\delta\, T_{\text{eff}} < 100$ K, $\delta \log g < 0.2$ dex, and δ[Fe/H] < 0.15 dex. Out of these, 2129 stars are found in the solar neighbourhood today. When taking into account the presence of 'intruders', i.e. stars that were born at inner Galactic radii but came closer to us because of radial migration, we find that $A(\text{Li})$ does not decrease when [Fe/H] exceeds solar, but rather stays roughly constant. This result is confirmed when considering the OC sample, thus strengthening previous results obtained using GES iDR5 by Randich et al. (2020). As noted by Romano et al. (2021), the field and OC subsamples lead to consistent results because our field star sample now includes warm stars younger than 2 Gyr: when these are missing, the recovered $A(^7\text{Li})$ versus [Fe/H] trend unavoidably suffers from the effects of some ^{7}Li depletion (see also Anthony-Twarog et al. 2018).

Furthermore, our sample allows us to trace the Galactic ^{7}Li gradient: the abundance of ^{7}Li is found to decline moderately from $A(^7\text{Li})\sim3.4$–3.5 to $A(^7\text{Li})\sim3.1$–3.2 when moving from the inner ($R_{\text{GC}} \simeq 5$ kpc) to the outer ($R_{\text{GC}} \simeq 15$ kpc) Galaxy (Romano et al. 2021, see also Randich et al. 2020).

Having assessed the $A(^7\text{Li})$ versus [Fe/H], age, and R_{GC} trends on observational grounds making use of the homogeneous GES iDR6 dataset, we turn to the theoretical interpretation of the observed trends. Romano et al. (2021) demonstrate that flatter or steeper theoretical relationships can be obtained in dependence of the adopted initial mass range for WD progenitors entering the formation of binary systems that lead to nova outbursts. From Fig. 1 it is seen that if the WD progenitors are in the range 3–8 $M_\odot$ the model predicts a milder increase of $A(^7\text{Li})$ in time (as traced by [Fe/H]) and a flatter $A(^7\text{Li})$ gradient, which seems to agree better with the observations. This would suggests

that more massive WDs are needed to obtain efficient ^{7}Li production during nova outbursts. We caution, however, that, although a decline of $A(^7\text{Li})$ for [Fe/H] > 0 is ruled out, the role of atomic diffusion in warm, metal-rich dwarf stars needs to be fully assessed before we can derive the actual ^{7}Li abundance at high metallicities (Charbonnel et al. 2021).

2.2. Evolution of neutron capture elements in dwarf galaxies

The majority of heavy elements beyond the iron peak originate via neutron capture. Neutron capture processes can be *slow* (s-process) or *rapid* (r-process) with respect to the β-decay in nuclei. These two processes require different astrophysical conditions, in terms of neutron density and temperature, and therefore they occur in different sites.

It has now been confirmed that the main s-process component takes place in the asymptotic giant branch (AGB) phase of low and intermediate mass stars (LIMS) (Busso et al. 1999), via the reaction $^{13}\text{C}(\alpha, \text{n})^{16}\text{O}$. The s-process can also occur in massive stars as a "weak" s-process (Langer et al. 1989; Prantzos et al. 1990), in this case the neutrons are produced through the reaction $^{22}\text{Ne}(\alpha, \text{n})^{25}\text{Mg}$.

On the other hand, the major astrophysical r-process site is still under debate, with possible candidate sites being supernovae or neutron star mergers (see e.g.: Thielemann et al. 2011; Frebel & Beers 2018; Cowan et al. 2019). For many years the occurrence of r-process has been associated with core-collapse supernovae (CC-SNe; Woosley et al. 1994; Horowitz 2012). However, the prompt explosion mechanism which was believed to eject extremely neutron-rich matter, has been completely ruled out by earlier hydrodynamical nucleosynthesis calculations. Simulations showed not only difficulties in reproducing the high entropy needed to reproduce the solar r-process abundances (Wanajo 2006; Arcones et al. 2007), but also that the neutrino winds which follow the supernovae explosion are only slightly neutron-rich or even proton-rich (Fröhlich et al. 2006; Fischer et al. 2010; Arcones & Thielemann 2013), providing insuf-

ficient conditions for the production of heavy r-process elements.

Among massive stars, CC-SNe induced by strong magnetic fields and/or fast rotation of the stellar core (magneto-rotational driven supernovae, MR-SNe) seem to also provide a source for the r-process (Winteler et al. 2012; Nishimura et al. 2015; Nishimura et al. 2017; Mösta et al. 2018; Halevi & Mösta 2018; Reichert et al. 2021). However, the required rotation rates and magnetic energies restrict the mechanism to a minority of progenitor stars: only 1% of all stars with initial mass larger than 10 M$_\odot$ may have the necessary conditions to host strong enough magnetic fields, according to Woosley & Heger (2006).

Merging neutron stars (MNS) have been supposed to be powerful sources of r-process matter and this has been proved thanks to the observation of the kilonova AT2017gfo, following the gravitational wave event GW170817 (Abbott et al. 2017; Watson et al. 2019). However, although both the r-process yields and the estimated rate of this phenomena seem to point towards MNS as the main r-process astronomical source, galactic chemical evolution models have problems to reproduce the r-process abundance pattern in the Galaxy if MNS are considered the only producers. Matteucci et al. (2014) introduced MNS in a chemical evolution model, showing that MNS can be the only r-process producers in the Galaxy, if a short and constant delay time for merging is adopted. If a more realistic delay time distribution (DTD) for merging is assumed (Simonetti et al. 2019; Côté et al. 2019; Molero et al. 2021b), then an additional r-process source must be included, especially at low metallicities. This is also in agreement with the large star-to-star heavy element abundance spread seen in observations at low metallicity (e.g., François et al. 2007; Hansen 2012).

With the goal of better understanding both the r- and s- process production sites at low metallicity, we study the chemical evolution of Eu, taken as a typical r-process element, and Ba abundances in 6 dwarf spheroidal galaxies (dSphs) and 2 Ultrafaint dwarf spheroidals (UFDs) for which homogeneous abundances have been published by Reichert et al. (2020).

We compute chemical evolution models in which we include LIMS as main s-process producers and test different scenarios for the production of Eu and r-process fraction of Ba: MNS and MRD-SNe. We use an updated version of the model presented by Lanfranchi & Matteucci (2004) to describe the chemical evolution of both UFDs and dSphs. Galaxies form by infall of primordial gas in a pre-existing diffuse dark matter (DM) halo. The model is one zone with instantaneous and complete mixing of gas. The stellar lifetimes are taken into account, thus relaxing the instantaneous recycling approximation (IRA). The model is able to follow the evolution of 31 chemical species, from H to Eu, during 14 Gyr.

In our simulations, MNS are systems of two $1.4M_\odot$ neutron stars with progenitors in the $9-50M_\odot$ mass range. In order to include the production of r-process elements from MNS in our chemical evolution code, we need to specify the following parameters (see Matteucci et al. 2014):

- the mass of each elements which is produced per merging event, Y_{Eu}^{MNS} and Y_{Ba}^{MNS};
- the time delay between the formation of the double neutron star system and the merging event, τ;
- the fraction of neutron stars in binaries that produce a MNS, α_{MNS}.

For what it concerns the yields of r-process elements from MNS, they have been obtained by assuming that there is a scaling relation between them and those of Sr. The adopted scaling factors are equal to 0.03 for Eu and to 3.16 for Ba, and have been found from the solar system r-process contribution, as determined by Simmerer et al. (2004). For the yields of Sr, we adopted the value found by Watson et al. (2019) in the reanalysis of the spectra of the kilonova AT2017gfo which followed the neutron-star merger GW170817, equal to $(1-5) \times 10^{-5}M_\odot$ Those yields have also been multiplied by two different factors (1×10^1, 1×10^2) in order to take into account the uncertainties that could affect them, because of their model assumptions as well as the scatter of Sr compared to Eu in old stars.

For the time delay τ, we adopt both a distribution of delay times (DTD) $\propto t^{-1}$ (see Simonetti et al. 2019 and Greggio et al. 2021 for a more detailed discussion) and a short and constant delay time for merging..

The parameter α_{MNS} is the probability of the MNS event. For a DTD with $\beta = -0.9$ it is equal to $\alpha_{MNS} = 5.42 \times 10^{-2}$ for spiral galaxies (Molero et al. 2021b). This value has been fixed in order to reproduce the observed present time MNS rate in the Milky Way as the one predicted by Kalogera et al. (2004), equal to $\sim 80^{+200}_{-60}\text{Myr}^{-1}$. It is reasonable to presume that in dwarf galaxies the present time rate of MNS is lower than the one in the Milky Way because of the lower SFR. Moreover, we adopted a lower probability of MNS in order to take into account the less efficient r-process material enrichment which characterizes dwarf galaxies. We set $\alpha_{MNS} = 2.15 \times 10^{-2}$ and based our consideration on the work of Bonetti et al. (2019), according to which in low mass galaxies neutron stars binary systems tend to merge with a large off-set from the host Galaxy, because of the kicks imparted by the two SN explosions. As stated by the authors, the immediate consequence of a merger location detached from the disc plane, is a dilution of the amount of r-process material retained by the Galaxy. For the production of r-process elements from MR-SNe, we select yields from Nishimura et al. (2017), their model L0.75. Finally, for the Ba s-process component, we have adopted yields of Busso et al. (2001) for LIMS of $(1.5-3.0)M_\odot$.

We have modelled the chemical evolution of 6 dSph and 2 UFD galaxies, which are: Böotes I (Boo I), Carina (Car), Fornax (For), Leo I (Leo), Reticulum II (Reticulum II), Sculptor (Scl), Sagittarius (Sgr) and Ursa Minor I (Umi I). Here we will focus on the results for Sculptor, representative of those obtained for all the other dSphs, and Reticulum II for it peculiar heavy elements abundances.

In Fig. 2 we report the observed [Eu/Fe] vs [Fe/H] pattern together with predictions of our models for Sculptor dSph. Observationally, the evolution of [Eu/Fe] vs [Fe/H] shows the typical trend of Eu in the Galaxy, similar to that of an α-element. We can easily distinguish

Table 1. Summary table of the nucleosynthesis prescriptions adopted by different models. In the 1st column in is reported the name of the model, in the 2nd column it is specified if there is production from MNS, in the 3rd it is specified if we adopted a DTD for MNS, in the 4th column it is reported the adopted yield of Eu from MNS, in the 5th column the yield of Ba from MNS, in the 6th it is specified if there is production from MRD-SNe, in the 7th column it is reported the yield of both Eu and Ba from MRD-SNe, in the 8th column the percentage of stars in the $(10-80)M_\odot$ mass range which explode as MRD-SNe and in the last column the range of metallicities in which the MRD-SNe channel is active for the Eu and/or Ba production.

| Model	MNS	DTD	Y_{Eu}^{MNS} ($M_\odot$)	Y_{Ba}^{MNS} ($M_\odot$)	MRD	$Y_{Eu,Ba}^{MRD}$	%	Z
C54	yes	no	$3.00\times10^{-5}-1.50\times10^{-4}$	$3.20\times10^{-4}-1.58\times10^{-3}$	no	–	–	–
C65	yes	no	$3.00\times10^{-6}-1.50\times10^{-5}$	$3.20\times10^{-5}-1.58\times10^{-4}$	no	–	–	–
C76	yes	no	$3.00\times10^{-7}-1.50\times10^{-6}$	$3.20\times10^{-6}-1.58\times10^{-5}$	no	–	–	–
CN65	yes	no	$3.00\times10^{-6}-1.50\times10^{-5}$	$3.20\times10^{-5}-1.58\times10^{-4}$	yes	Nishimura et al. (2017) L0.75	1	all
DN65	yes	yes	$3.00\times10^{-6}-1.50\times10^{-5}$	$3.20\times10^{-5}-1.58\times10^{-4}$	yes	Nishimura et al. (2017) L0.75	1	all
DN65Z	yes	yes	$3.00\times10^{-6}-1.50\times10^{-5}$	$3.20\times10^{-5}-1.58\times10^{-4}$	yes	Nishimura et al. (2017) L0.75	1	$<10^{-3}$
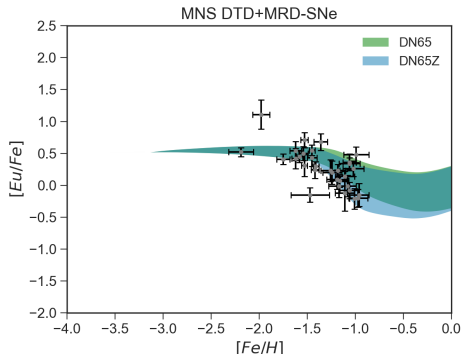
Fig. 2. Results of models for the [Eu/Fe] vs [Fe/H] pattern for Sculptor dSph. Eu is produced both by MNS with a DTD and MRD-SNe acting both at low Z and and for all the range of metallicities. Figure from Molero et al. (2021a).

the plateau at low to intermediate metallicities (from ~ -2.25 to ~ -1.25 dex) and the decrease at higher [Fe/H]. We show results of models DN65 and DN65Z in which both MNS with a DTD and MRD-SNe can produce Eu. For both models the yield of Eu from MNS is in the $(3.0\times10^{-6}-1.5\times10^{-5})M_\odot$ range, while that of MRD-SN is equal the one of Nishimura et al. (2017). Models are shown as a shaded area with the upper limit corresponding to the model with the higher yield of Eu and the lower limit to the model with the lower one. For clarity, the prescriptions for our different models

are reported in Table 1. The two models differ only for the range of metallicities in which MRD-SNe are active: in model DN65 they act for the whole range, while in model DN65Z they act only at low metallicities. Both models seems to be able to reproduce the main trend. In particular, the lack of Eu from MNS at low metallicities, due to longer delay times for merging, is compensated by the production of Eu from MRD-SN which, in both models, are active at low metallicities. In the same way, when in model DN65Z MRD-SNe stop to produce Eu from metallicities higher than 10^{-3}, MNS can compensate. For model DN65 we get Eu from both MNS and MRD-SNe also at high metallicities, resulting in a slightly higher trend with respect to model DN65Z.

In Fig. 3, we report predictions for the [Ba/Fe] vs [Fe/H] together with the observational data. The observed [Ba/Fe] vs [Fe/H], is characterized by a low abundance of Ba at low metallicities ([Fe/H]≤-2.25) and by almost solar values from intermediate to high metallicities, suggesting different mechanisms for the production of the s- and r- process fractions of Ba. In fact, at low metallicities Ba is mostly created by r-process, but as more LIMS go through the AGB phase, the s-process becomes more important and the [Ba/Fe] ratio increases with increasing [Fe/H] until a plateau is reached (Skúladóttir et al. 2020). We show results of models CN65 and DN65 in which r-process Ba and Eu are produced by both MRD-SNe and MNS. As for 2, models are shown as
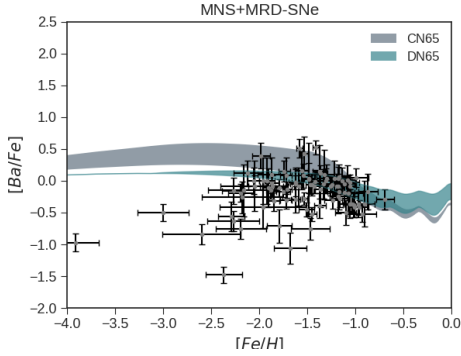
Fig. 3. Results of models for the evolution of [Ba/Fe] vs [Fe/H] for Sculptor dSph. r-process Ba is produced both by MRD-SNe and by MNS (with and without a DTD) while s-process Ba production comes from LIMS. Figure from Molero et al. (2021a).

shaded areas, with the upper limit corresponding to the higher yield of Ba and the lower limit to the lower one. In model CN65 we assume a short and constant delay time for MNS, while in model DN65 a DTD is adopted. As expected, both models are not able to reproduce the low data of [Ba/Fe] at low metallicities. For both models, in fact, the production of r-process Ba sets in too early and a too high trend is produced at low [Fe/H].

In Figure 4 we report our results together with the observational data for the [Eu/Fe] vs [Fe/H] in the Reticulum II UFD. Concerning the observational data, Reticulum II stands out among all the other galaxies because of its peculiar Eu and Ba abundances. The data are concentrated at low metallicities and also show strong enhancements, which is about 2 orders of magnitude higher than what is observed in the other galaxies. The generally accepted explanation for the high r-process abundances observed in Reticulum II is that a single nucleosynthetic event produced a large quantity of r-process material (Ji et al. 2016). Therefore, in our model we increased the value of the $\alpha_{\rm MNS}$ parameter to 1 in order to artificially obtain a total of 1 event of MNS in the first Gyr of SF of Reticulum II. A probability of 100% of having a MNS event is a strong condition, but

it is justified by the low stellar mass content of Reticulum II ($\sim 10^3$ $M_\odot$). We then computed the [Eu/Fe] and the [Ba/Fe] vs [Fe/H] abundances for the three sets of yields. The results are shown in Fig. 4. As one can see, the observational data can be reproduced by models which assume r-process yields similar to those of the other dwarfs (rather than higher). In particular, the yields can be in the $(1.50-3.00)\times10^{-6} M_\odot$ range for Eu and around $1.50 \times 10^{-5} M_\odot$ for Ba.

It is reasonable to presume that a possible scenario is one in which NS merge with a DTD and produce Eu together with MRD-SNe. In this case, MRD-SNe can produce Eu at all metallicities or only at low ones, without making any significant difference in the final results. This allows us to reproduce the [Eu/Fe] vs [Fe/H] abundances, in agreement with what has been proposed by several authors (e.g.: Simonetti et al. 2019; Côté et al. 2019; Skúladóttir & Salvadori 2020; Molero et al. 2021b). In particular, the amount of Eu produced by each MNS event would be in the $(3.0 \times 10^{-6} - 1.5 \times 10^{-5}) M_\odot$ range, while that produced by MRD-SNe would be in the range of the theoretical calculations of Nishimura et al. (2017) and equal to $4.69 \times 10^{-7} M_\odot$. Here we assume that only 1% of all stars with initial mass in the $(10-80) M_\odot$ range would explode as MRD-SNe (according also to Woosley & Heger 2006). However, within this scenario the low metallicity data of [Ba/Fe] cannot be reproduced. The only way to reproduce them is if only MNS (with DTD) are producing the r-process fraction of Ba, with yields in the $(3.20 \times 10^{-5} - 1.58 \times 10^{-4}) M_\odot$ range. If also MRD-SNe participate to this process, the agreement with the data is lost. Nevertheless, excluding MRD-SNe from the production of Ba cannot be physical motivated.

For Reticulum II scenario is different from those for the other galaxies, because of the peculiar r-/s-process elements pattern which characterizes this Galaxy. At the moment, the most common accepted theory is that a single nucleosynthetic event polluted the Galaxy at early times with copious amount of r-process material. We therefore computed a test in which the rate of MNS was forced to be equal
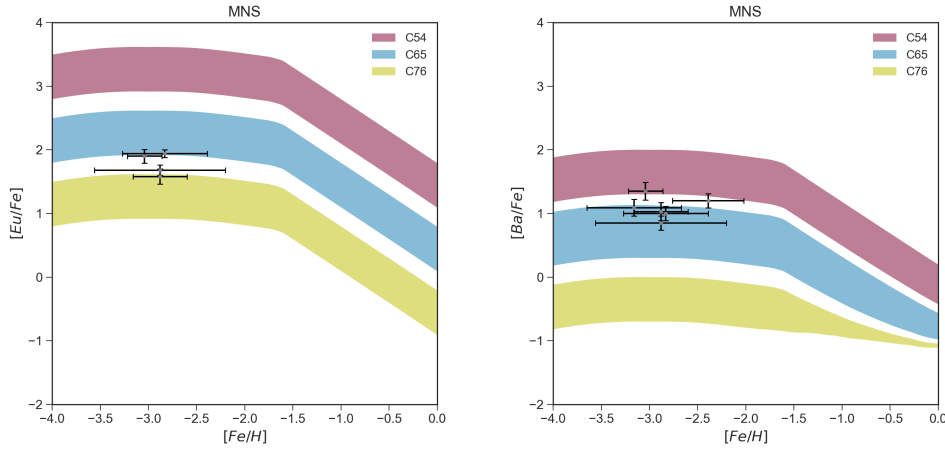
Fig. 4. Results of models C54, C65 and C76 for Reticulum II for [Eu/Fe] and [Ba/Fe] vs [Fe/H] in the case of 1 event of MNS in the first Gyr. Figure from Molero et al. (2021a).

to 1 in the first Gyr of SF. This allowed us to adopt realistic r-process yields, similar to those obtained for other dwarfs/UFDs. In order to obtain such a rate of MNS we had to set $\alpha_{MNS} = 1$, namely we had to assume a probability of 100% of having a MNS event. This is a strong assumption, but which can be justified by the low stellar mass content of Reticulum II.

2.3. Chemical evolution of radioactive nuclei: ^{26}Al & ^{60}Fe

^{26}Al and ^{60}Fe are two short-lived radioactive nuclei with decay time of τ_{26Al}=1.05 Myr and τ_{60Fe}=3.75 Myr, respectively. Their main producers are massive star with short lifetime, therefore these nuclei are abundant in those regions which have suffered a recent event of star formation.

Since 1991, the γ-survey COMPTEL collected evidences of the flux coming from the decay of ^{26}Al and observed ~2 M$_\odot$ of ^{26}Al within 5 kpc from the Galactic centre (Diehl et al. 1995). Later, from 2002 the γ-survey INTEGRAL performed the same measurements and confirmed the earlier COMPTEL results, having observed a mass of ^{26}Al in the range 1.8–3.6 M$_\odot$ within 5 kpc from the

Galactic centre (Diehl2013). In addition it observed the flux ratio ^{60}Fe, which is ~15% ± 5% of that of ^{26}Al.

Chemical evolution models are useful tools to offer theoretical constraints on observational data, and in case of unavailable data, they can perform predictions. The majority of the models used until now to study radioactive isotopes are analytical models (Clayton 1984, 1988), where restrictive hypothesis such as a single burst of star formation and instantaneous recycling approximation are assumed.

In this study we used a numerical chemical evolution code (as done by Timmes et al. 1995) to study the evolution of ^{26}Al and ^{60}Fe in the Milky Way, comparing several sets of yields for massive stars and for nova systems (only for ^{26}Al). Our model describes the Galaxy as composed of concentric rings 2 kpc wide, homogeneously mixed without exchange of matter among them. The innermost region (R<2 kpc) represents the bulge. The formation of the disc is described by a double infall law, where the first infall formed the thick disc and the second formed the thin disc on a longer timescale. We assumed a Kennicutt (1998) SFR and a Kroupa et al. (1993) IMF. For the bulge we assumed a single infall on a short timescale,
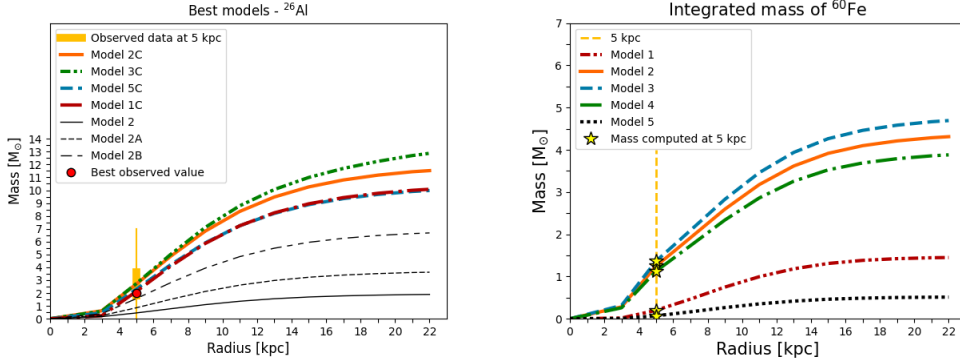
Fig. 5. *Left panel*: mass of ^{26}Al as a function of Galactocentric radius. The four colored models (green, orange, red and blue) are those compatible with the observations (yellow thick line). The three black lines are examples of non-compatible models. The best observational value is represented by the red dot. We consider as best model the red one, which assumes yields by Woosley & Weaver (1995) for massive stars and high contribution from novae. *Right panel*: mass of ^{60}Fe as a function of Galactocentric radius. The lines represent the five different models tested and the stars show the value each model predicts at 5 kpc from the Galactic centre. Figure from Vasini et al. (2022).

a Kennicutt (1998) SFR and a Salpeter (1955) IMF. The model consider production by SNII, SNIb, SNIc, SNIa and nova systems. The fundamental chemical evolution equation studies how the composition of the ISM changes considering the effects of star formation, injection of elements from dying stars, infall and radioactive decay. With these prescription, our model can reproduce the main features of the Galaxy, such as the surface density of gas, the total mass and the fraction of stars, the present rates of SNII, SNIa and novae and the infall rate.

We tested stellar yields for massive stars by Woosley & Weaver (1995) metallicity dependent and at solar metallicity, Limongi & Chieffi (2006) at solar metallicity and Limongi & Chieffi (2018) metallicity and rotation dependent. We also tested, only for ^{26}Al, three sets of nova system yields, one by José & Hernanz (1998) and two by José & Hernanz (2007), and the case of no contribution from novae. For ^{26}Al, we combined the four models of massive star yields with the four models for nova systems, for a total of sixteen models tested. For ^{60}Fe we have only the five models for massive stars (Limongi & Chieffi 2006) offer two sets

for ^{60}Fe, one assuming Schwarzschild convection criterion, one assuming Ledoux convection criterion).

For both isotopes we computed the mass as a function of Galactocentric radius (0–22 kpc) and the present time injection rate (the present time rate at which ^{26}Al and ^{60}Fe are injected in the ISM at the stellar death). We compared the masses with observations by INTEGRAL and the injection rates with the previous theoretical result by Timmes et al. (1995).

For ^{26}Al mass, among the sixteen models tested, only four were compatible with the observed range 1.8.–3.6 $M_\odot$ within 5 kpc from the Galactic centre. The left panel of Fig. 5 shows the four compatible models (the colored ones) which overlap with the observed range (yellow thick band) together with some examples of non compatible ones (black models). The best model assumes yields by Woosley & Weaver (1995) metallicity dependent and produces 2.12 $M_\odot$ within 5 kpc. We selected this one since is the closest to the best observational value, ∼2 $M_\odot$ (red dot). It is noteworthy that all the compatible models have a high contribution coming from novae, therefore without
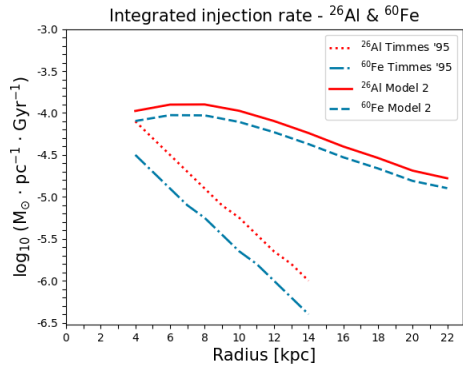
Fig. 6. Present time injection rates as a function of Galactocentric radius (solid red line and dashed blue line) compared with the results by Timmes et al. (1995) (dotted red line and dash-dotted blue line). Our results are larger and the maximum is located in the region 5-7 kpc, whereas the older results had a maximum in the centre of the Galaxy. Figure from Vasini et al. (2022).

nova systems it is not possible to reproduce the observations.

For ^{60}Fe mass we compared our results to estimates obtained from flux observation (it is important to stress that they are uncertain), which state that ^{60}Fe should lie in the range 0.9-1.8 $M_\odot$. We have only one model compatible, which assumes yields by Limongi & Chieffi (2006) with Schwarzschild convection criterion and predicts ~1 $M_\odot$ within 5 kpc from the Galactic centre, and is shown in the right panel in Fig. 5.

Regarding the injection rates, we compared the results by Timmes et al. (1995) with our models (we selected those with the same nucleosynthesis prescriptions). The results are shown in Fig. 6: we obtain higher injection rates with a maximum located in the region 5–7 kpc, in agreement with the maximum of the present time star formation, whereas in Timmes et al. (1995) the maximum was located in the inner part of the Galaxy.

In this section, we studied the chemical evolution of ^{26}Al and ^{60}Fe in the Galaxy by means of a numerical model whose prescriptions reproduce the present features of the Milky Way. We estimated ~2.12 $M_\odot$ ^{26}Al within 5 kpc from the Galactic centre with a high contribution coming from nova systems. We stress that without nova production the data can not be reproduced. Regarding ^{60}Fe we estimate its mass to be ~1 $M_\odot$ within 5 kpc from the Galactic centre. We also computed the present time injection rates for both elements. With respect of the previous results by Timmes et al. (1995) our injection rates are larger and peaked in the region 5–7 kpc as we expected considering the present time star formation.

2.4. Impact of rotational yields of massive stars in the evolution of the Milky Way Galaxy

The massive stars ($\geq 11 M_\odot$) evolve on shorter time than low mass stars and explode as Supernova Ib/c +II. They end their evolution as stellar remnant of black hole or Neutron star. Due to the short lifetime of massive stars, their contribution to the chemical enrichment of the ISM is very significant. The changes in the yields of the massive stars can have a strong influence on the chemical evolution of the Galaxy. The rotational yields of the massive stars provided by Limongi & Chieffi (2018)for a wide range of mass and metallicity are used in the present work. Due to the conservation of the angular momentum, massive stars can have a large rotational velocity at the time of their formation in the molecular cloud. The presence of rotation induces instabilities during various phases of stellar evolution. These instabilities further enhance the Internal mixing of stellar material and eventually can result in higher neutron production and other effects.

The Galactic chemical evolution models presented here understand the influence of Nucleosynthetic yields of massive stars in the Galaxy's chemical evolution. The GCE models developed in this work are based on the theoretical and simulation framework developed in Sahijpal & Kaur (2018) based upon the the Monte Carlo technique. Instead of solving the classical non-linear integro-differential equations Matteucci & Francois (1989); Chiappini et al. (1997), we have adopted a direct ap-

proach of physically evolving the Galaxy realistically Alibés et al. (2001); Sahijpal & Gupta (2013). The Galaxy forms by the accretion of the infalling intergalactic gas from which the stars form according to the adopted SFR and IMF at each simulation time step of 1 Myr. The Monte Carlo approach is used especially for incorporating SN Ia population synthesis based on random numbers, which is explained extensively in detail in (Sahijpal & Kaur 2018). In these GCE models, the Galaxy is divided into 8 rings of 2 kpc each from 2-18 kpc. The two-infall accretion process forms the Galaxy's Halo-thick disc and thin disc over a galactic time scale. The halo-thick disc phase formed in the fast accretion phase within the initial 1 Gyr, and the thin disc formed over a longer time scale known as inside out scenario (Chiappini et al. 1997; Sahijpal & Kaur 2018; Micali et al. 2013). In the solar neighbourhood the surface mass density is considered to be 51 $M_\odot pc^{-2}$ (Bovy & Rix 2013). The stars in the mass range 0.1–100 $M_\odot$ formed from the accreted matter at each time step of 1 Myr as per the stellar birth rate function, which constitutes star formation rate (SFR) and initial mass function (IMF). We considered Schmidt-Kennicutt SFR law (Kennicutt 1998). The power law exponent in IMF is considered to be 0 and 1.7 in the mass range of 0.1–1 and 1–100 $M_\odot$ stars, respectively. To understand the influence of rotation and different explosion mechanisms of the massive stars(>11$M_\odot$), we simulated four GCE models with two sets of nucleosynthetic yields from Woosley & Weaver (1995) and Limongi & Chieffi (2018). We focus on nucleosynthetic yields of massive stars with stellar rotational velocities, 0, 150 and 300 kms^{-1} from Limongi & Chieffi (2018), which are used in the GCE models namely LC-0, LC-150 and LC-300, respectively. The GCE models produced by yields from Woosley & Weaver (1995) are named WW-0. The major assumption mentioned by Limongi & Chieffi (2018) is that they consider only neutron capture and beta decay for stable and unstable isotopes around the magic numbers with N= 82 and 126 and all other intermediate isotopes are at the local equilibrium. The overall gas, stellar and total luminous matter is evaluated in each model

and agrees with the observed data. For all four GCE models, the stellar yields of low and intermediate stars in the mass range of 0.8-8 $M_\odot$ and the SN Ia data are used from (Karakas & Lattanzio 2007) and (Iwamoto et al. 1999) respectively.

The results for the G-dwarf distribution for the four models are shown in Fig. 7 for the four annular rings, viz., 4–6 kpc, 8–10 kpc, 10–12 kpc and 12–14 kpc. The G-dwarf metallicity distribution for the Galaxy is computed by monitoring the evolution of stars in the mass range of 0.8–1.25 $M_\odot$. The observational data across 3–15 kpc from the Galactic centre over a distance of |z| < 0.5 kpc from the Galactic plane is taken from Hayden et al. (2015). The predicted trends show significant deviation from the observed profile in the low metallicity regime ([Fe/H] ≤ 0.5).

This could be partially due to our limited observational data usage over |z| < 0.5 kpc from the Galactic plane (Hayden et al. 2015), which excludes the higher |z| values. The predicted peaks match the observations across the Galaxy except for the inner region of the Galaxy. Because of the different yield sets used, each GCE model follows a different evolution history, and the impact can be seen in the G-dwarf distribution in the Galaxy. Overall, the predicted peak values in regions > 8 kpc agree with the observed MDF (Hayden et al. 2015) for all four models. Out of the non-rotational models, WW-0 and LC-0, the highest G-dwarfs are observed for the model WW-0 at all galactocentric radii. The predicted G-dwarf distribution for WW-0 model exhibit sharper peaks in comparison to the LC-0 model. The impact of the stellar rotational yields is not significant in explaining the G-dwarf distribution in the Galaxy compared to the non-rotating stellar model by Limongi & Chieffi (2018). Among the rotational models, LC-300 shows higher peaks than LC-150 at all distances. In the 4–6 kpc region, the peak for the LC-150 model is significantly displaced to the higher metallicity value, making it most disagree with the observations.

The disagreement in the lower metallicity part of the distribution could be attributed to the higher assumed value of the total surface

mass density in the models. Lower values of total surface mass density could lead to the lower production of G-dwarf stars in the early period of Galaxy formation. The deviation from the Gaussian distribution is also seen in the observed data by Hayden et al. (2015) in the mid-plane of inner and the outer regions of the Galaxy. The metallicity distribution function is observed to be negatively and positively skewed in the inner and outer Galaxy, respectively. However, the GCE model predictions are heavily negatively skewed in all over the Galaxy. One of the most plausible reasons for this behaviour can be the stellar radial migration, which is not incorporated in these GCE simulations.

3. Conclusion

The GCE models discussed above predict the chemical history of the Milky Way Galaxy and other dwarf galaxies. The overall predictions of the 1–D GCE models give a reasonable explanation for the abundance trends of various elements by incorporating different features like episodic infall of gas, inside–out formation of the disc, gas density–dependent star formation and gas outflows etc. The predictions of GCE models include many observed galactic features, i.e. abundance gradient, inversion in abundance gradients at high red–shift and bi–modality in age–metallicity relations etc., for a range of low, intermediate and heavy elements.

More data with better age estimates and from different parts of the Galaxy provides better constraints for GCE model predictions. As discussed in section 2.1, the spectroscopic information of OCs with the GES iDR6 provided a detailed view of the ^{7}Li distribution in the Galaxy. The ^{7}Li abundance trends as a function of metallicity and galactocentric distance are presented and compared with the GCE model predictions. The GCE models suggest the Nova outbursts as the primary producer of the galactic ^{7}Li. The OC sample used here spans a wide range of galactocentric distances, 5 kpc $\leq R_{GC} \leq$ 15 kpc. The ^{7}Li gradient traced by OCs ranges from $A(^7$Li$)\sim$3.4–3.5 to $A(^7$Li$)\sim$3.1–3.2 dex from the inner to the outer disc (Romano et al. 2021).

Further in section 2.2, the GCE models to predict the chemical evolution of the neutron capture elements in the local group dwarf galaxies and ultra dwarf galaxies are discussed. These models investigate the r-process nucleosynthesis by testing different nucleosynthesis prescriptions for merging neutron stars (MNS) and magneto-rotational driven supernovae (MRD-SNe). For Sculptor and Fornax, GCE models can predict the [Eu/Fe] vs [Fe/H] by having a constant and short delay for merging or MRD-SNe. Also, the Ba abundance trends are in good agreement in the case of the GCE models, where r-process elements are produced only with longer delays, namely by MNS with a DTD. However, the results of the GCE models for abundance trends Ba and Eu together show some disagreement with the observations. It is indicated that the nucleosynthesis contribution of the r and s process to various galaxies modelled here needs further investigation.

Further, section 2.3 discussed the GCE models for unstable nuclides, ^{26}Al and ^{60}Fe, throughout the Milky Way Galaxy. GCE models dealing with the Short-lived radionuclides are essential to understand the Gamma–ray observations. Also, ^{60}Fe and ^{26}Al from Massive stars inside a stellar cluster give clues to the origin of the Solar System (Kaur & Sahijpal 2019). These models included the nucleosynthesis yields from massive stars, AGB stars, and SNIa. Also, the stellar yields of ^{26}Al were considered from Novae as well. The best fit GCE models can predict the mass of ^{26}Al in the range of 1.8–3.6 $M_\odot$ as observed in Gamma–ray observations within inner 5 kpc of the Galaxy. The results suggest that irrespective of the massive star's yields, the Nova contribution is very significant to the ^{26}Al production in the Galaxy. The LIMs and SNIa yields have little impact on the predicted mass of the ^{26}Al in the Galaxy. The model with massive stars yields from Limongi & Chieffi (2006) also produces the ^{60}Fe in the mass range of 0.9 – 1.8 $M_\odot$, which is indirectly computed from the ^{60}Fe/^{26}Al flux ratios. The models also predict the maximum injection rate's location to be around 5–7 kpc in the Galaxy.
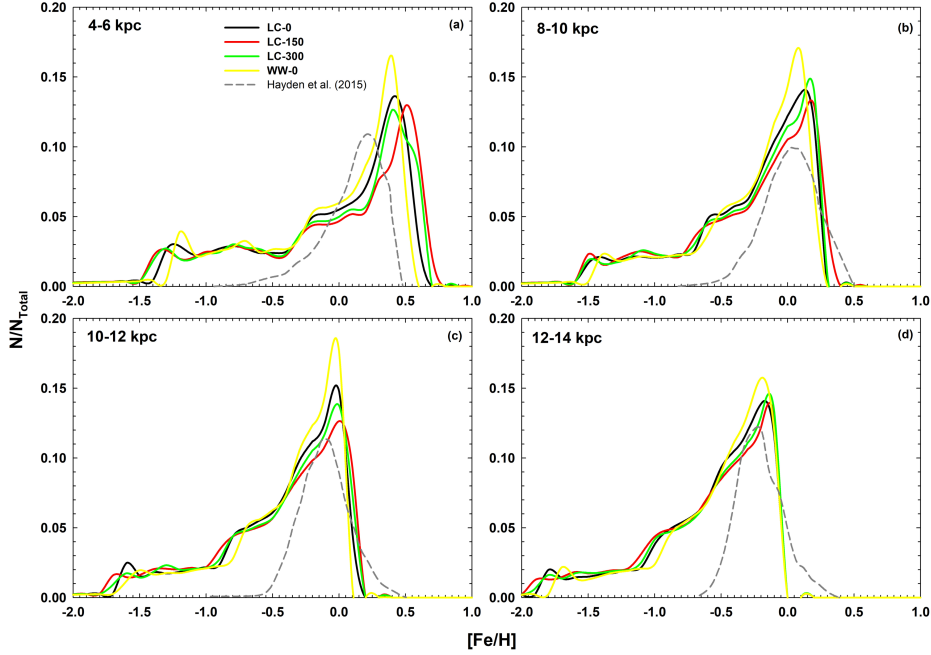
Fig. 7. The predicts trends for G-dwarf metallicity distribution for rotational and non-rotational yields GCE models, LC-0, LC-150, LC-300, and WW-0, in the annular ring at a) 4–6 kpc, b) 8–10 kpc, c) 10–12 kpc, and d) 12–14 kpc of the Galaxy at 13.8 Gyr. The G-dwarf metallicity distribution is computed by monitoring the evolution of stars in the mass range of 0.8–1.25 $M_\odot$. The observational data is taken from Hayden et al. (2015) over a distance of |z| < 0.5 kpc from the Galactic plane. The annular rings of 2 kpc widths defined by Hayden et al. (2015) initiate at a distance of 3 kpc from the Galactic centre instead of 2 kpc assumed in the present work. Figure from Kaur (2020).

We have discussed the impact of the rotational yields on the chemical evolution of the Milky Way Galaxy in section 2.4. These GCE models aim to study the influence of the distinct sets of non-rotational stellar yields from Woosley & Weaver (1995) and Limongi & Chieffi (2018). The impact of the Yields of massive stars with different rotational velocities from Limongi & Chieffi (2018) on the evolutionary history of the Galaxy is also studied. The GCE model predictions for G–dwarf distribution show a significant deviation from the observed profile in the low metallicity regime ([Fe/H] < -0.5). The results suggest that there is little impact of the different evolutionary history of the Galaxy on G-dwarf distribution of the Galaxy in all four models with rotating and non-rotating sets of massive stars yields (Kaur 2020).The overall deviation of the predicted G-dwarf distribution from the observations in the low metallicity regime might arise from the high surface mass density of gas in the early period of the Galaxy formation. The values of the total surface mass density is considered to vary from 110 to 0.41 $M_\odot pc^{-2}$ for thick disc and 267 to 3.4 $M_\odot pc^{-2}$ for thin disc in the Galaxy from 2–18 kpc. However, we also computed the total gas mass in the Galaxy, and it is $(6.8-7.0) \times 10^9$ $M_\odot$ which is in agreement with the values of 7×10^9 $M_\odot$ (Bovy & Rix 2013) and $(8.1 \pm 4.5) \times 10^9$ $M_\odot$ (Kubryk et al. 2015). The observed deviation also could be the result of the stellar migration in the Galaxy. The low mass stars with long life spans are subjected

to significant distance because of stellar migration. The GCE models presented here do not consider stellar migration between the different annular rings in the Galaxy.

References

Abbott, B. P., Abbott, R., Abbott, T. D., et al. 2017, ApJ, 850, L40

Alibés, A., Labay, J., & Canal, R. 2001, A&A, 370, 1103

Anthony-Twarog, B. J., Lee-Brown, D. B., Deliyannis, C. P., & Twarog, B. A. 2018, AJ, 155, 138

Arcones, A., Janka, H. T., & Scheck, L. 2007, A&A, 467, 1227

Arcones, A. & Thielemann, F. K. 2013, Journal of Physics G Nuclear Physics, 40, 013201

Asplund, M., Grevesse, N., Sauval, A. J., & Scott, P. 2009, ARA&A, 47, 481

Bonetti, M., Perego, A., Dotti, M., & Cescutti, G. 2019, MNRAS, 490, 296

Bonifacio, P. & Molaro, P. 1997, MNRAS, 285, 847

Bovy, J. & Rix, H.-W. 2013, ApJ, 779, 115

Burkert, A., Truran, J. W., & Hensler, G. 1992, ApJ, 391, 651

Busso, M., Gallino, R., Lambert, D. L., Travaglio, C., & Smith, V. V. 2001, ApJ, 557, 802

Busso, M., Gallino, R., & Wasserburg, G. J. 1999, ARA&A, 37, 239

Charbonnel, C., Borisov, S., de Laverny, P., & Prantzos, N. 2021, A&A, 649, L10

Chiappini, C., Gratton, & R. 1997, The Astrophysical Journal, 477, 765

Chiappini, C., Matteucci, F., & Romano, D. 2001, The Astrophysical Journal, 554, 1044

Clayton, D. D. 1984, ApJ, 285, 411

Clayton, D. D. 1988, MNRAS, 234, 1

Côté, B., Eichler, M., Arcones, A., et al. 2019, ApJ, 875, 106

Cowan, J. J., Sneden, C., Lawler, J. E., et al. 2019, arXiv e-prints, arXiv:1901.01410

D'Antona, F. & Matteucci, F. 1991, A&A, 248, 62

Delgado Mena, E., Bertrán de Lis, S., Adibekyan, V. Z., et al. 2015, A&A, 576, A69

Diehl, R., Dupraz, C., Bennett, K., et al. 1995, A&A, 298, 445

Fischer, T., Thielemann, F. K., & Liebendörfer, M. 2010, in American Institute of Physics Conference Series, Vol. 1269, 10th International Symposium on Origin of Matter and Evolution of Galaxies: OMEG - 2010, ed. I. Tanihara, H. J. Ong, A. Tamii, T. Kishimoto, T. Kajino, S. Kubono, & T. Shima, 181–188

François, P., Depagne, E., Hill, V., et al. 2007, A&A, 476, 935

Frebel, A. & Beers, T. C. 2018, Physics Today, 71, 30

Fröhlich, C., Hix, W. R., Martínez-Pinedo, G., et al. 2006, New Astronomy Reviews, 50, 496

Fu, X., Romano, D., Bragaglia, A., et al. 2018, A&A, 610, A38

Gaia Collaboration, Brown, A. G. A., Vallenari, A., et al. 2021, A&A, 649, A1

Gaia Collaboration, Prusti, T., de Bruijne, J. H. J., et al. 2016, A&A, 595, A1

Gilmore, G., Randich, S., Asplund, M., et al. 2012, The Messenger, 147, 25

Greggio, L. 2005, A&A, 441, 1055

Greggio, L., Simonetti, P., & Matteucci, F. 2021, MNRAS, 500, 1755

Grisoni, V., Matteucci, F., Romano, D., & Fu, X. 2019, MNRAS, 489, 3539

Guiglion, G., Chiappini, C., Romano, D., et al. 2019, A&A, 623, A99

Guiglion, G., de Laverny, P., Recio-Blanco, A., et al. 2016, A&A, 595, A18

Halevi, G. & Mösta, P. 2018, MNRAS, 477, 2366

Hansen, C. J. 2012, arXiv e-prints, arXiv:1212.4496

Hayden, M. R., Bovy, J., Holtzman, J. A., et al. 2015, ApJ, 808, 132

Horowitz, C. J. 2012, arXiv e-prints, arXiv:1212.6405

Iwamoto, K., Brachwitz, F., Nomoto, K., et al. 1999, ApJS, 125, 439

Izzo, L., Della Valle, M., Mason, E., et al. 2015, ApJ, 808, L14

Ji, A. P., Frebel, A., Chiti, A., & Simon, J. D. 2016, Nature, 531, 610

José, J. & Hernanz, M. 2007, Journal of Physics G Nuclear Physics, 34, R431

Kalogera, V., Kim, C., Lorimer, D. R., et al. 2004, ApJ, 601, L179

Karakas, A. & Lattanzio, J. C. 2007, PASA, 24, 103

Karakas, A. I. 2010, MNRAS, 403, 1413

Kaur, T. 2020, PhD thesis, Department of Physics, Punjab University, http://hdl.handle.net/10603/331671

Kaur, T. & Sahijpal, S. 2019, MNRAS, 490, 1620

Kennicutt, Robert C., J. 1998, ApJ, 498, 541

Kobayashi, C. & Nakasato, N. 2011, ApJ, 729, 16

Koeppen, J. & Arimoto, N. 1990, A&A, 240, 22

Kroupa, P. 1998, in Astronomical Society of the Pacific Conference Series, Vol. 134, Brown Dwarfs and Extrasolar Planets, ed. R. Rebolo, E. L. Martin, & M. R. Zapatero Osorio, 483

Kroupa, P., Tout, C. A., & Gilmore, G. 1993, MNRAS, 262, 545

Kubryk, M., Prantzos, N., & Athanassoula, E. 2015, A&A, 580, A126

Lanfranchi, G. A. & Matteucci, F. 2004, MNRAS, 351, 1338

Langer, N., Arcoragi, J. P., & Arnould, M. 1989, A&A, 210, 187

Limongi, M. & Chieffi, A. 2006, ApJ, 647, 483

Limongi, M. & Chieffi, A. 2018, ApJS, 237, 13

Lodders, K., Palme, H., & Gail, H. P. 2009, Landolt Börnstein, 4B, 712

Matteucci, F. 2001, The chemical evolution of the Galaxy, Vol. 253 (Springer Science & Business Media)

Matteucci, F. 2021, The Astronomy and Astrophysics Review, 29, 1

Matteucci, F., D'Antona, F., & Timmes, F. X. 1995, A&A, 303, 460

Matteucci, F. & Francois, P. 1989, MNRAS, 239, 885

Matteucci, F., Romano, D., Arcones, A., Korobkin, O., & Rosswog, S. 2014, MNRAS, 438, 2177

Micali, A., Matteucci, F., & Romano, D. 2013, MNRAS, 436, 1648

Minchev, I., Chiappini, C., & Martig, M. 2013, A&A, 558, A9

Molero, M., Romano, D., Reichert, M., et al. 2021a, MNRAS, 505, 2913

Molero, M., Simonetti, P., Matteucci, F., & della Valle, M. 2021b, MNRAS, 500, 1071

Mösta, P., Roberts, L. F., Halevi, G., et al. 2018, ApJ, 864, 171

Nishimura, N., Sawai, H., Takiwaki, T., Yamada, S., & Thielemann, F. K. 2017, ApJ, 836, L21

Nishimura, N., Takiwaki, T., & Thielemann, F.-K. 2015, ApJ, 810, 109

Pagel, B. E. 2009, Nucleosynthesis and chemical evolution of galaxies (Cambridge University Press)

Pardi, M. C., Ferrini, F., & Matteucci, F. 1995, ApJ, 444, 207

Pasquini, L., Avila, G., Blecha, A., et al. 2002, The Messenger, 110, 1

Pitrou, C., Coc, A., Uzan, J.-P., & Vangioni, E. 2018, Phys. Rep., 754, 1

Prantzos, N. & Aubert, O. 1995, A&A, 302, 69

Prantzos, N., de Laverny, P., Guiglion, G., Recio-Blanco, A., & Worley, C. C. 2017, A&A, 606, A132

Prantzos, N., Hashimoto, M., & Nomoto, K. 1990, A&A, 234, 211

Randich, S., Gilmore, G., & Gaia-ESO Consortium. 2013, The Messenger, 154, 47

Randich, S., Pasquini, L., Franciosini, E., et al. 2020, A&A, 640, L1

Reichert, M., Hansen, C. J., Hanke, M., et al. 2020, A&A, 641, A127

Reichert, M., Obergaulinger, M., Eichler, M., Aloy, M. Á., & Arcones, A. 2021, MNRAS, 501, 5733

Romano, D., Magrini, L., Randich, S., et al. 2021, A&A, 653, A72

Romano, D., Matteucci, F., Molaro, P., & Bonifacio, P. 1999, A&A, 352, 117

Romano, D., Matteucci, F., Ventura, P., & D'Antona, F. 2001, A&A, 374, 646

Sahijpal, S. & Gupta, G. 2013, M&PS, 48, 1007

Sahijpal, S. & Kaur, T. 2018, Monthly Notices of the Royal Astronomical Society, 481, 5350

Salpeter, E. E. 1955, ApJ, 121, 161

Scalo, J. M. 1986, Fund. Cosmic Phys., 11, 1

Simmerer, J., Sneden, C., Cowan, J. J., et al. 2004, ApJ, 617, 1091

Simonetti, P., Matteucci, F., Greggio, L., & Cescutti, G. 2019, MNRAS, 486, 2896

Skúladóttir, Á., Hansen, C. J., Choplin, A., et al. 2020, A&A, 634, A84

Skúladóttir, Á. & Salvadori, S. 2020, A&A, 634, L2

Spite, F. & Spite, M. 1982, A&A, 115, 357

Steigman, G. 2007, Annual Review of Nuclear and Particle Science, 57, 463

Thielemann, F. K., Arcones, A., Käppeli, R., et al. 2011, Progress in Particle and Nuclear Physics, 66, 346

Timmes, F., Woosley, S., & Weaver, T. A. 1995, The Astrophysical Journal Supplement Series, 98, 617

Travaglio, C., Randich, S., Galli, D., et al. 2001, ApJ, 559, 909

Vasini, A., Matteucci, F., & Spitoni, E. 2022, MNRAS, 517, 4256

Wakker, B. P., Howk, J. C., Savage, B. D., et al. 1999, Nature, 402, 388

Wanajo, S. 2006, The Astrophysical Journal, 650, L79

Watson, D., Hansen, C., Selsing, J., et al. 2019, Nature, 574, 497

Winteler, C., Käppeli, R., Perego, A., et al. 2012, ApJ, 750, L22

Woosley, S. E. & Heger, A. 2006, ApJ, 637, 914

Woosley, S. E. & Weaver, T. A. 1995, ApJS, 101, 181

Woosley, S. E., Wilson, J. R., Mathews, G. J., Hoffman, R. D., & Meyer, B. S. 1994, ApJ, 433, 229